Materials Transactions, Vol. 43, No. 8 (2002) pp. 2130 to 2136

Influence of Shear Height on Shear Strength of Tin-Lead Solder Ball Bonding

Takashi Nakamori[1], Mayumi Ikeda[2,*], Kunihiro Noguchi[2,*], Isao Shimizu[2] and Yasuhide Ohno[2]

[1]*Nippon Steel Corp., Otemachi, Tokyo 100-8071, Japan*
[2]*Department of Materials Science and Engineering, Faculty of Engineering, Kumamoto University, Kumamoto 860-0862, Japan*

The crack generation energy U_1 and the crack progress energy U_2 of eutectic Sn–37 mass%Pb solder ball and Sn–36 mass%Pb–2 mass%Ag one were surveyed by the shear test. Both balls were bonded at various reflow cooling rates (10–200 K/min). The shear test was carried out under the condition of two kinds of the shear height, $Z = 0\,\mu m$ and $Z = 200\,\mu m$. U_1 and U_2 were calculated by multiplying the shear strength by the shear distance. Though U_2 was independent on the cooling rate, the ball composition and the shear height, U_1 changed depending on these parameters. Only U_1 of Sn–36 mass%Pb–2 mass%Ag ball bonding cooled at 200 K/min dropped sharply though U_1 of both ball bonding was almost the same and increased with the faster cooling rates in case of $Z = 0\,\mu m$. U_1 of Sn–36 mass%Pb–2 mass%Ag ball bonding was higher than that of the eutectic ball at each cooling rate as a result of the shear test at $Z = 200\,\mu m$. The needle shape Ag_3Sn intermetallic compound in Sn–36 mass%Pb–2 mass%Ag ball and near the interface contributed mainly to the lower U_1 at $Z = 0\,\mu m$ because Ni_3Sn_4 reaction layer formed at 200 K/min was thin. The higher U_1 at $Z = 200\,\mu m$ was due to the fine lamellar structure (Sn phase/Pb phase) in Sn–36 mass%Pb–2 mass%Ag ball. The shear property of the same ball depended on the shear height in the present study.

(Received January 31, 2002; Accepted June 17, 2002)

Keywords: *tin-lead-silver ball, cooling rate, reaction layer, intermetallic compound, shear strength, crack generation energy, crack progress energy*

1. Introduction

Ball grid array (BGA) technique is a bonding process which solder balls are arranged on Cu pads in a print board and heated in a reflow instrument after setting IC chips on them.[1–4] This process makes semiconductor devices higher integrated, smaller, thinner and lighter than conventional ones. Recently, IC devices trend to be much more integrated and complicated by the progress of BGA technique. Though the bonding has been performed in the air or nitrogen atmosphere, it is difficult that the correct and uniform thermal control on the print board is achieved. The thermal distribution on the same print board changes following the device density. The different melting or solidification rate leads to the reduction of the bonding property and durability. Therefore, it is important to survey the effect of the cooling rate and the ball composition to the bonding microstructure and the strength because such data can give the information how the reflow have been carried out. These results could conduct the actual reflow situation and further the best reflow condition. The database on the microstructure and the strength of the ball bonding has been collected.[5–13] One of the experimental procedures for estimating the bonding property is a shear test. But each test has been performed by each researcher under the quite different condition such as shear speed, shear height and so on. The quite different feature could be obtained with the same apparatus and the same ball composition. So the systematic data about the shear test of the ball bonding is needed. The shear tests of eutectic Sn–37 mass%Pb ball bonding and Sn–36 mass%Pb–2 mass%Ag one have been carried out under the condition of two kinds of the shear height ($Z = 0\,\mu m$ and $Z = 200\,\mu m$). The crack generation energy U_1 and the crack progress energy U_2 were calculated by analyzing the shear curves. The influence of the shear height on the shear strength is reported in the present study.

2. Experimental Procedure

Solder balls used in this study were Sn–37 mass%Pb (described 37Pb later) and Sn–36 mass%Pb–2 mass%Ag (described 36Pb2Ag later) supplied by Nittetsu Micro Metal Co. The diameter of both balls was approximately 600 μm. The height of the balls from the resist layer surface after the bonding was approximately 570 μm. The compact furnace (Japan High Tech Co) was attached on the stage of an optical microscopy. Each ball was put on each Cu pad on the print board (square $10 \times 10\,mm^2$) with a tweezers after the common flux liquid was applied on the Cu pads. The print board was set into the furnace. The Cu pads were covered with 4 μm thick Ni–P electroless plating layer and Au vaporize layer with approximately 0.1 μm. Ball melting appearance was monitored on TV during the reflow. The other reflow conditions (heat speed, holding period, cooling method and so on) have been reported already.[12] The shear test was performed as follows. The shear height Z was fixed at 0 μm and 200 μm from the print board surface as showed in Fig. 1. The shear speed was 2.7 mm/s. The shear value of each specimen was estimated by the average of at least 20 times trials. For investigating the fracture mechanism, an electronic measuring instrument (NR-2000, Keyence Co) which can record simultaneously the shear strength change gained with a shear tester as the voltage wave was applied. The sampling capacity and the high resolution for the input signal of this apparatus are 400 kHz and 14 bit, respectively. The raw data was analyzed by converting the voltage into the shear strength with a software (Wave Shot, Keyence Co) on a personal computer. The hardness of the ball was measured by the micro Vickers

*Graduate Student, Kumamoto University.

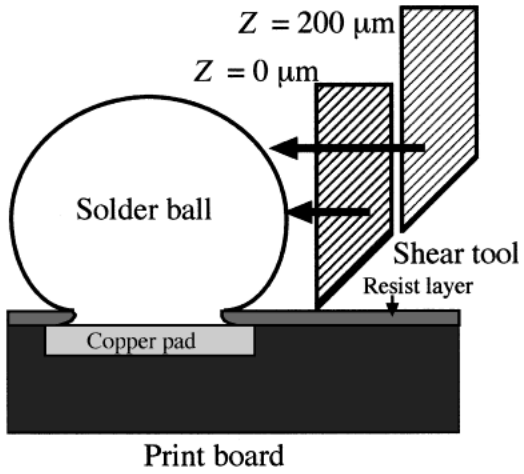

Fig. 1 Illustration of shear test at shear height $Z = 0\,\mu m$ and $Z = 200\,\mu m$.

hardness test (load; 0.05 N, time; 15 s). The hardness value was estimated by the average of 10 times trials. The ball surface and cross sectional observation was performed with a scanning electron microscopy (SEM, accelerative voltage; 20 kV). A transmission electron microscopy (TEM, accelerative voltage; 200 kV) and EDX were used for characterizing the microstructure of the ball bonding. TEM specimen was prepared with the microtome.[14,15]

3. Results and Discussion

3.1 Shear curve of the ball bonding

Figure 2 shows shear curves of 37Pb ball bonding tested at the shear height $Z = 0\,\mu m$. Figures 2(a), (b) and (c) indicate the results of reflow cooling rates 200 K/min, 100 K/min and 10 K/min, respectively. The vertical axis is the shear strength and the transverse axis is the shear period. Each curve is a representative one which was gained an average shear strength value. The shear strength value is expressed in each figure. Though there is naturally no signal of shear strength until the contact between the shear tool and the ball surface occurs, the curves rise slowly when the tool touches the ball surface. The curves reach the maximum value at the stage when the crack generates in the ball or at the bonding interface. This period is confined as t_1 in the present study. Therefore, the crack generation energy U_1 is measured as the integration from the initial strength to the maximum. The strength descends for the shorter time compared to t_1. The period spent from the maximum strength to 0 N is confined as t_2. The crack progress energy U_2 is estimated as the integration from the maximum strength to 0 N. From Fig. 2, t_1 and the maximum strength decrease at 10 K/min though t_2 has no change. The curve shape at the cooling rates is very gentle. Figure 3 shows shear curves of 36Pb2Ag ball bonding tested at the shear height $Z = 0\,\mu m$. Figures 3(a), (b) and (c) show the results of reflow cooling rates 200 K/min, 100 K/min and 10 K/min, respectively. Since the strength fluctuations when the shear tool tip rubs the print board surface can not be seen in Fig. 2 and Fig. 3, the effect of the contact between the tool tip and the board surface on the shear strength is neglected at $Z = 0\,\mu m$. The curve shape at the slower cooling rate 10 K/min is sharper than that at the faster cooling rate 200 K/min. That means

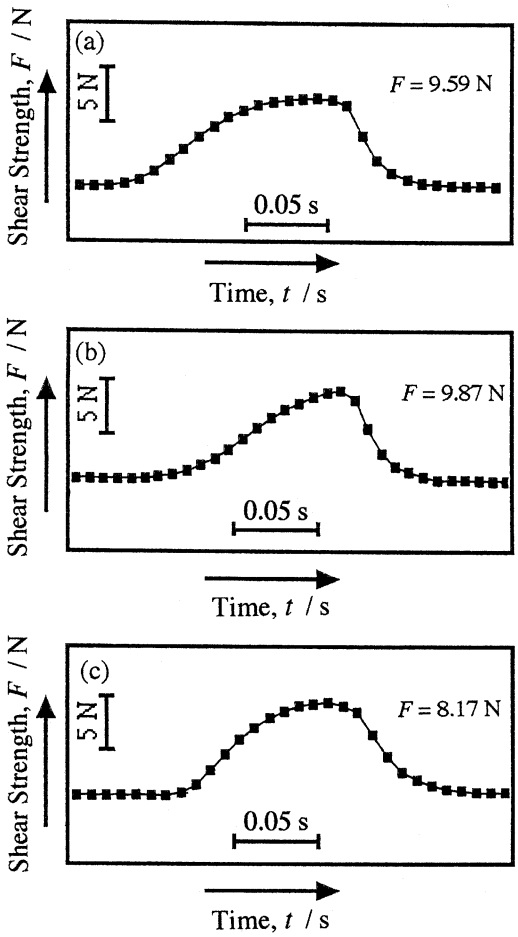

Fig. 2 Shear curve of Sn37Pb ball bonding cooled at 200 K/min (a), 100 K/min (b) and 10 K/min (c) by shear test at $Z = 0\,\mu m$.

the crack generated faster on the bonding cooled at 10 K/min. Figure 4 shows shear curves tested under the condition of $Z = 200\,\mu m$. Figures 4(a), (b) and (c) show the result of 37Pb ball bonding cooled at 200 K/min, 100 K/min and 10 K/min, respectively. The curve shape of Fig. 4(c) is clearly sharper than other ones. The shear strength cooled at 10 K/min is lower than any other ones cooled at the faster cooling rates. The fracture may occur abruptly in the shorter period. Figures 5(a), (b) and (c) show shear curves of 36Pb2Ag ball bonding tested at shear height $Z = 200\,\mu m$. Each curve shows the result of reflow cooling rates 200 K/min, 100 K/min and 10 K/min, respectively. It is notable that there is no change in the curve shapes of the bonding cooled at 200 K/min to 10 K/min compared to 37Pb ball bonding results. Especially, the shear curve tested for the bonding cooled at 10 K/min is gentle and t_2 is longer at the slower cooling rates.

3.2 Crack generation and progress periods

The period of the crack generation t_1 and the one of the crack progress t_2 measured by the shear test which was performed at the shear height $Z = 0\,\mu m$ are shown in Fig. 6. The transverse axis in both Figs. 6(a) and (b) indicates the cooling rate. It is apparent that t_1 of 36Pb2Ag ball bonding is shorter than that of 37Pb one at each cooling rate (Fig. 6(a)). That means the crack of 36Pb2Ag ball bonding generated easier than that of 37Pb ball. On the contrary, t_2 of 36Pb2Ag ball

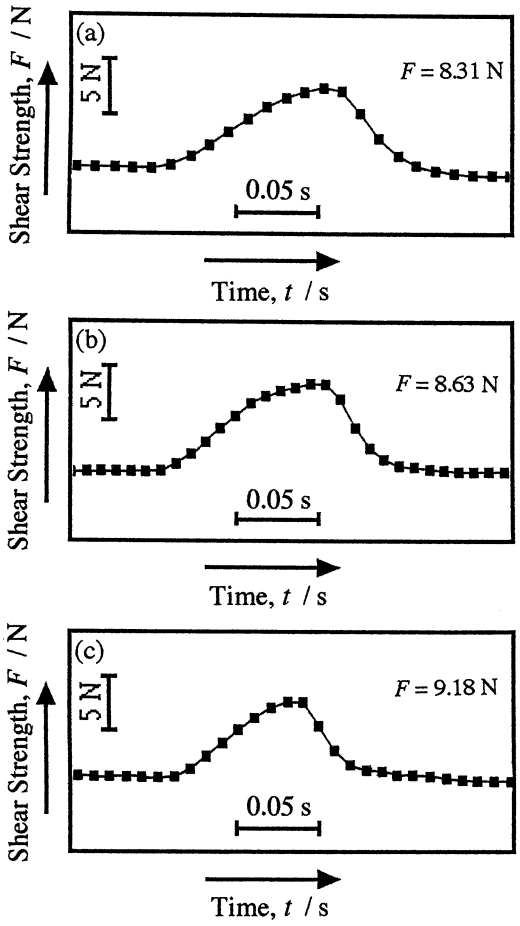

Fig. 3 Shear curve of Sn36Pb2Ag ball bonding cooled at 200 K/min (a), 100 K/min (b) and 10 K/min (c) by shear test at $Z = 0\,\mu m$.

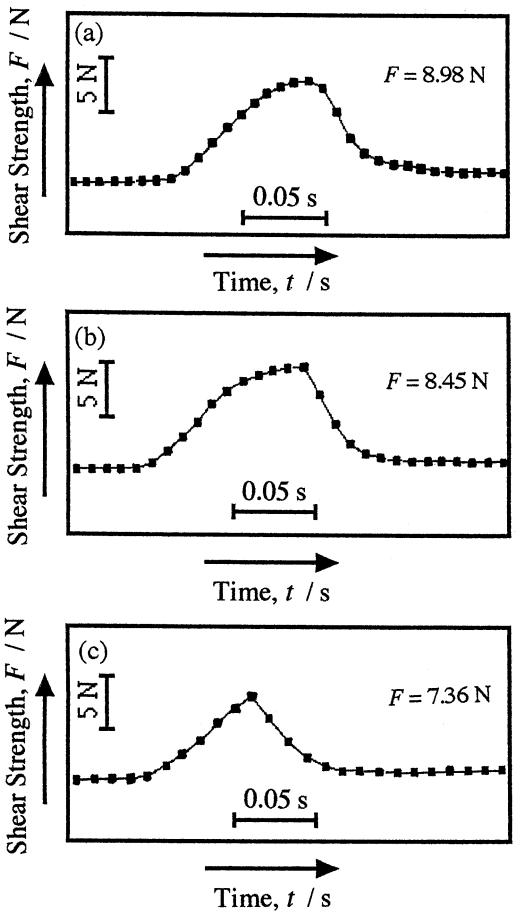

Fig. 4 Shear curve of Sn37Pb ball bonding cooled at 200 K/min (a), 100 K/min (b) and 10 K/min (c) by shear test at $Z = 200\,\mu m$.

bonding is the same compared to that of 37Pb one at each cooling rate (Fig. 6(b)). The crack progress behavior does not depend on the ball composition in case of $Z = 0\,\mu m$. Since the shear tool speed was too fast in this study, the crack might advance easily once it generated. The various shear speed must be considered. Figure 7 shows t_1 and t_2 measured by the shear test which was performed at the shear height $Z = 200\,\mu m$. It is conspicuous that the opposite result is obtained compared with Fig. 6(a). The crack generation period t_1 of 36Pb2Ag ball bonding is longer than that of 37Pb one at the cooling rates. There is no change about t_1 in both balls at 100 K/min and 200 K/min. However there is the strict descend at 10 K/min. The mechanical property of a ball itself could influence on the initial shear property until the crack occurs by the shear test at $Z = 200\,\mu m$. Figure 8 shows SEM micrograph of the 36Pb2Ag ball bonding cooled at 10 K/min which was deformed by the shear test at $Z = 200\,\mu m$. The tool transferred to approximately 100 µm from the contact point on the ball surface at the shear velocity, 0.17 mm/s. The wavy deformation of the ball without the interface crack is observed as pointed by the arrow in Fig. 8. This shear speed (0.17 mm/s) is approximately 0.063 times slower compared with the shear one (2.7 mm/s) described in the present experimental procedure. However, the very initial deformation behavior could be reflected to the ball deformation sheared at the shear speed of the present study. The result in Fig. 7 can conduct that the microstructure and the mechanical property of the ball itself will be effective to the initial shear behavior. The crack progress period t_2 of both balls is almost the same at each cooling rate as shown in Fig. 7(b).

3.3 Relation of crack generation, progress energy and microstructure

Figure 9 shows the crack generation energy U_1 (black plot in Fig. 9) and the crack progress energy U_2 (white plot in Fig. 9) of both balls at $Z = 0\,\mu m$ in each cooling rate. U_1 and U_2 were calculated as follows:

$$U_1 = \sum (dFs_1 \times dLs) \tag{1}$$

$$U_2 = \sum (dFs_2 \times dLs) \tag{2}$$

$$dLs = hs \times dt \tag{3}$$

Where dFs_1 and dFs_2 are the shear strength for the short span dt subdivided t_1 and t_2 in Fig. 2 to Fig. 5, respectively. The transfer distance of the shear tool dLs is a value multiplied the shear speed hs by dt as expressed the eq. (3). Since the shear speed hs was 2.7 mm/s and dt was 0.01 s in this study, dLs is 0.027 mm. Therefore, U_1 and U_2 are computed with the eqs. (1), (2) and (3) as follows.

$$U_1 = 0.027 \times \sum dFs_1 \tag{4}$$

$$U_2 = 0.027 \times \sum dFs_2 \tag{5}$$

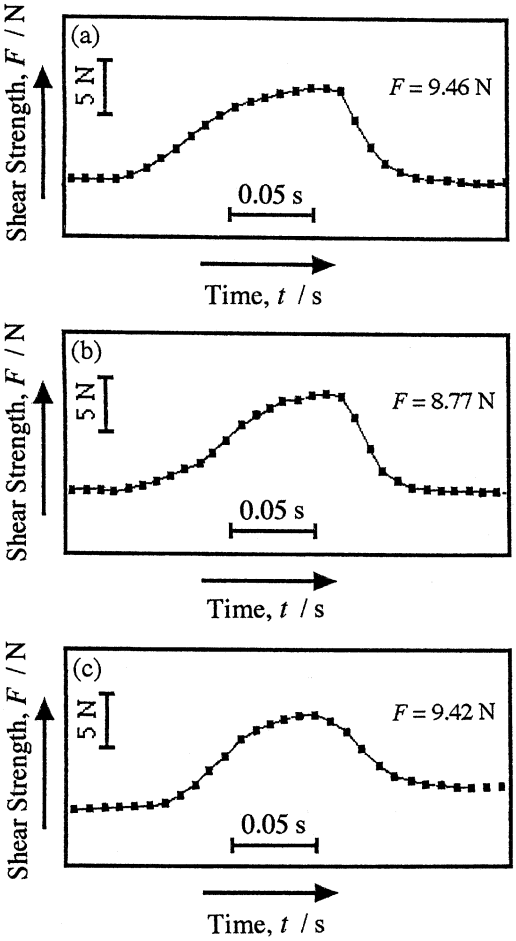

Fig. 5 Shear curve of Sn36Pb2Ag ball bonding cooled at 200 K/min (a), 100 K/min (b) and 10 K/min (c) by shear test at $Z = 200\,\mu m$.

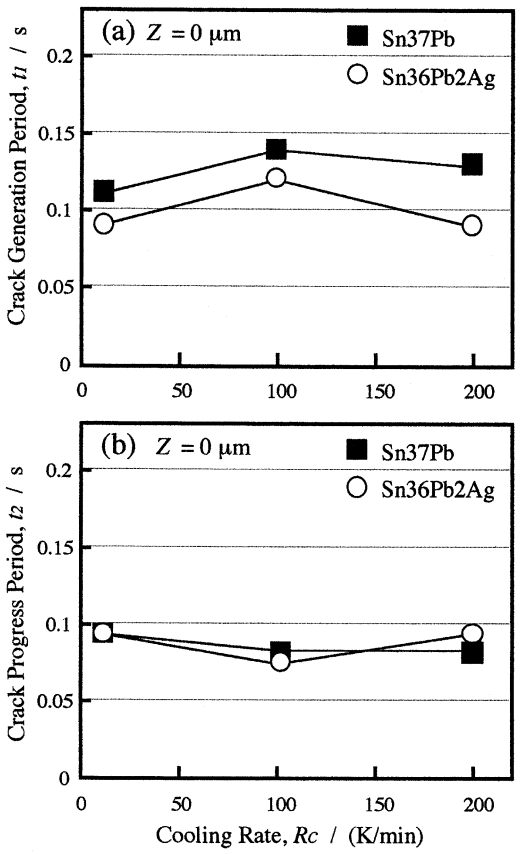

Fig. 6 Relation of crack generation period (a), crack progress period (b) and cooling rate by shear test at $Z = 0\,\mu m$.

From Fig. 9, U_1 of 37Pb ball bonding rises at the faster cooling rates. U_1 of 36Pb2Ag ball bonding also rises until 100 K/min, however these values are a bit lower than that of 37Pb one. It is outstanding that U_1 of 36Pb2Ag one decreases markedly at 200 K/min. Since U_1 reflects to the shear force and instructs the ball and the bonding interface mechanical property, the bigger U_1 conducts that the crack does not generate easier. Figure 10 shows TEM micrograph (a) of 36Pb2Ag ball bonding interface cooled at 100 K/min and the results of EDX analysis of the area B (b) and C (c) in (a). The column structure is a Ni_3Sn_4 intermetallic compound because Sn and Ni are detected in the column area by the rate of 4 to 3 (Fig. 10(b)). Ni_3Sn_4 might form by reacting between Sn in the ball and Ni which diffused from Ni–P electroless plating layer. Only Ni is detected in the area C in (a) under the column structure (Fig. 10(c)). Though P amount in Ni–P electroless plating layer was not clear, P might concentrate in the electroless plating layer by Ni diffusion to the ball.[13] Such microstructure has been reported by many researchers. Cu detected in Ni_3Sn_4 and Ni phase as shown in Fig. 10(b) and (c) is from Cu mesh.[15] The column Ni_3Sn_4 intermetallic compound was observed on all ball bonding interfaces in the present study. The Ni_3Sn_4 layer thickness of both balls increased at the lower cooling rate.[13] The bigger Ni_3Sn_4 layer thickness contributed to U_1 descent at the lower cooling rates in Fig. 9. Figures 11(a) and (b) show a TEM bright field image

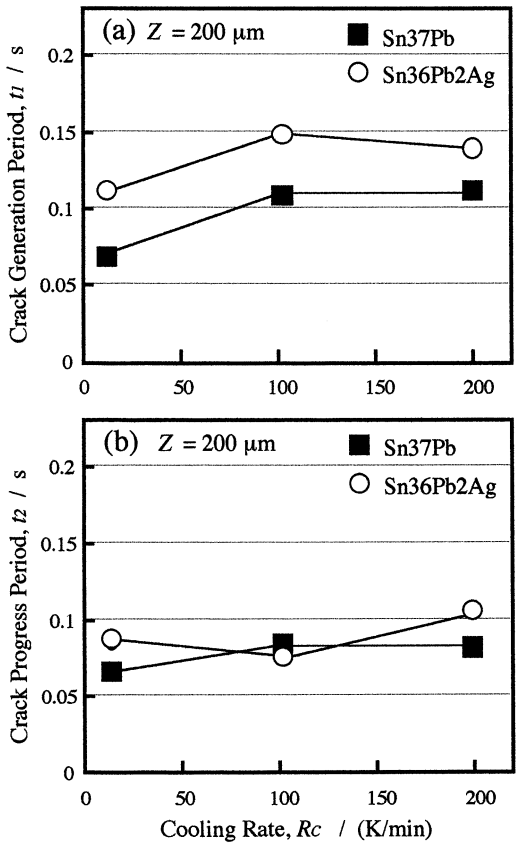

Fig. 7 Relation of crack generation period (a), crack progress period (b) and cooling rate by shear test at $Z = 200\,\mu m$.

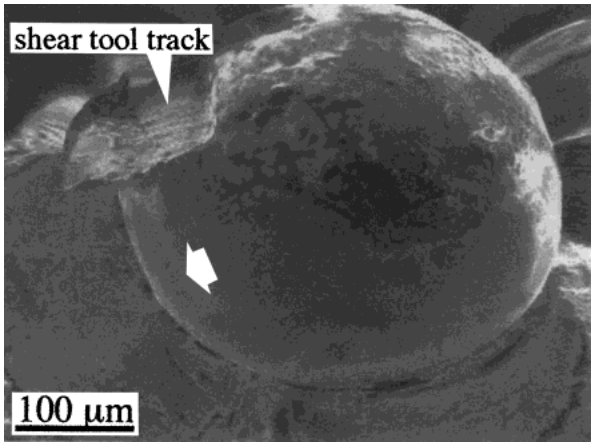

Fig. 8 SEM micrograph of Sn36Pb2Ag ball bonding cooled at 10 K/min after the shear test.

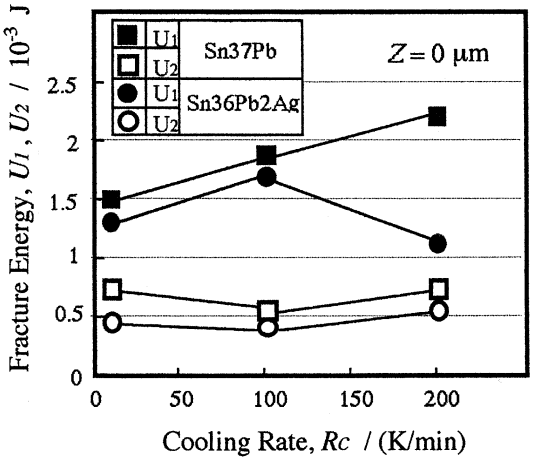

Fig. 9 Relation of cooling rate and fracture energy by shear test at shear height $Z = 0\,\mu$m.

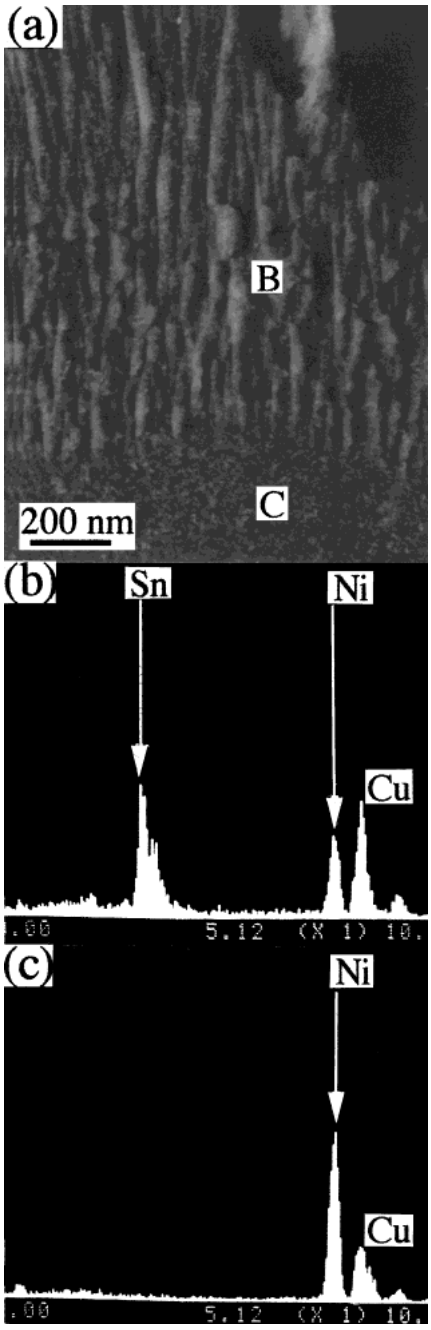

Fig. 10 TEM micrograph of Sn36Pb2Ag ball bonding interface cooled at 100 K/min (a) and result of EDX analysis of the area B (b) and C (c) in (a).

of 36Pb2Ag ball cooled at 200 K/min and an electron diffraction pattern from the area B in (a). EDX analysis results of the area B and C in Fig. 11(a) are shown in Figs. 11(c) and (d). There are many glass-like phases (arrows in Fig. 11(a)) in the eutectic structure. It is considered that they are amorphous phases because the hallow ring was obtained in the glass-like phases as shown in Fig. 11(b). From Fig. 11(c), oxygen and carbon are detected with Sn and Pb in the amorphous phase. On the contrary, there is no oxygen and carbon except Sn in the area C of Fig. 11(a). The amorphous phases formed in the solder balls have not been reported before. Oxygen and carbon might dissolve from the flux liquid to the solder during the melting and be included in the ball without volatilizing at the faster cooling. The amorphous phases were also observed in near neck parts of the ball bonding. They might become the crack origin and induce the drastic U_1 descent of 36Pb2Ag ball cooled at 200 K/min. Figure 12 shows a SEM micrograph and an illustration of Ag_3Sn needle shape intermetallic compound (arrows in Fig. 12) in 36Pb2Ag ball cooled at 200 K/min.[13] Though Ag_3Sn precipitates have been observed in 36Pb2Ag ball at each cooling rate, the brittle precipitate could strictly influence the shear property in case of the thinner Ni_3Sn_4 layer at 200 K/min. U_2 of both ball bonding is lower than U_1 and is almost the same value in contradiction on U_1. Since U_2 expresses the energy of the crack propagation, the same value indicates that the crack propagates with no difference in both ball bonding. Figure 13 shows the crack generation energy U_1 (black plot in Fig. 13) and the crack progress energy U_2 (white plot in Fig. 13) of both balls at $Z = 200\,\mu$m. U_1 of both balls tends to decrease as the cooling rate becomes lower. The remarkable differences about U_1 can be seen compared to the result of Fig. 9. U_1 at $Z = 200\,\mu$m of 36Pb2Ag ball bonding cooled at 200 K/min is higher than that at $Z = 0\,\mu$m. Figure 14 shows the result of hardness test on both balls. Micro Vickers hardness test was carried out on the ball (Fig. 14(a)) and Knoop hardness test was carried out on the bonding interface (Fig. 14(b)). The hardness of the 36Pb2Ag ball and the interface is higher than that of 37Pb ones. It was due to the fine lamellar struc-

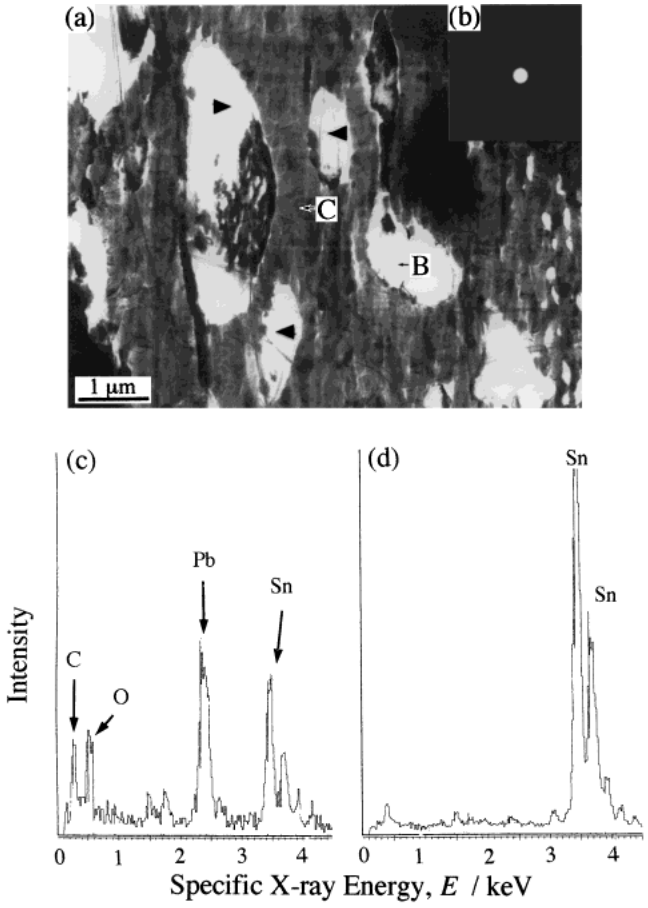

Fig. 11 TEM micrograph of Sn36Pb2Ag ball cooled at 100 K/min (a), electron diffraction pattern (b) of the area B in (a) and result of EDX analysis of the area B (c) and C (d) in (a).

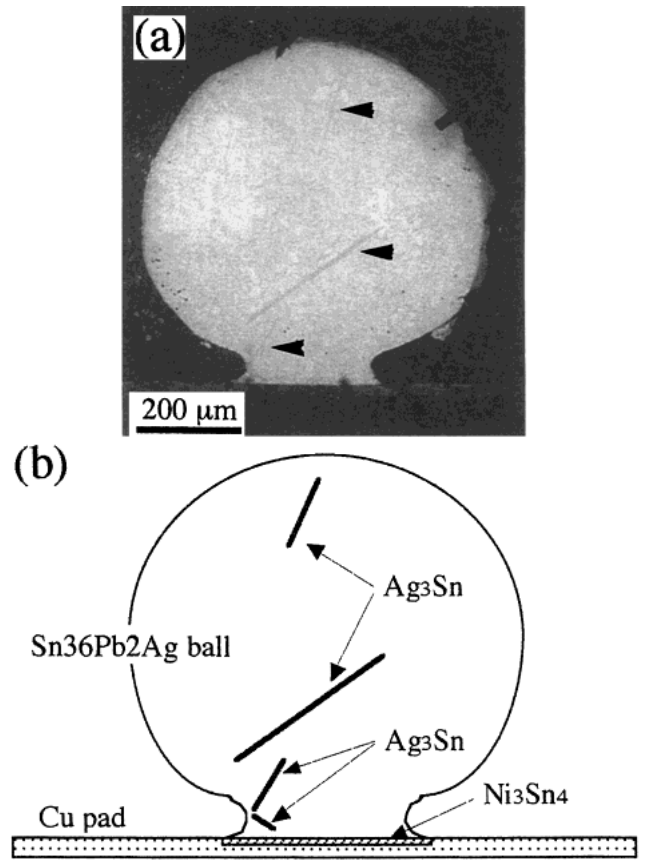

Fig. 12 SEM micrograph (a) and illustration (b) of Sn36Pb2Ag ball bonding cooled at 200 K/min.

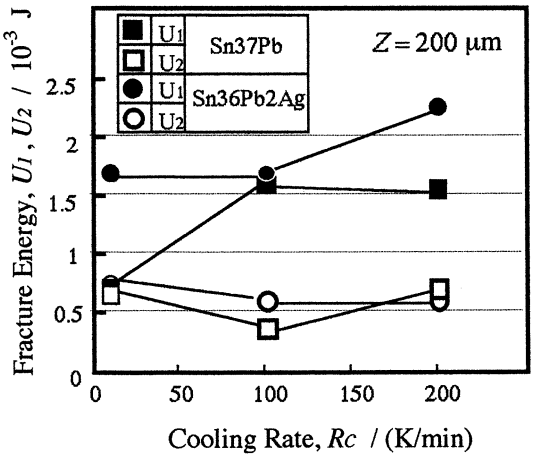

Fig. 13 Relation of cooling rate and fracture energy by shear test at shear height $Z = 200\,\mu m$.

ture (Sn phase/Pb phase) formed by the rapid cooling.[13] It can be thought that the higher ball mechanical property contributed to the higher U_1 at 200 K/min in case of $Z = 200\,\mu m$ because the shear tool transformed the ball mainly until the crack generated. The minute lamella could play the role of the shock absorber when the shear tools collided to the ball surface. U_1 at $Z = 200\,\mu m$ of 37Pb ball bonding is lower than that at $Z = 0\,\mu m$. The bigger moment in the bonding interface might be loaded since the force point (the tool contact area) is so far from the action point (the edge of the bonding). Therefore U_1 at $Z = 200\,\mu m$ of 37Pb ball bonding decreased compared with that at $Z = 0\,\mu m$ since the bigger moment forced to the solder ball and interface. There is no change U_2 at each cooling rate in Fig. 13. The crack progress behavior is independent of the cooling rates, the ball composition and the shear height in the present study. There was no difference in the crack progress behavior between 37Pb ball bonding and 36Pb2Ag one once the crack generated. That is because the needle-shape Ag_3Sn in 36Pb2Ag ball did not form enough densely to obstruct the crack progress though it could be an origin of the crack generation.

4. Conclusions

The shear test of Sn–37Pb and Sn–36Pb–2Ag ball bonding cooled at 10 K/min to 200 K/min has been carried out under the condition of two kinds of the shear height ($Z = 0\,\mu m$ and $Z = 200\,\mu m$). The crack generation energy U_1 and the crack progress energy U_2 were calculated by analyzing the shear curves. The influence of the shear height on the shear strength investigated in the present study is described as follows.

(1) U_1 depended on the cooling rate, the ball composition and the shear height.

(2) U_1 at $Z = 0\,\mu m$ of both ball bonding cooled at 10 K/min and 100 K/min was almost the same but U_1 of Sn–36Pb–2Ag ball bonding cooled at 200 K/min sharply decreased.

(3) The needle shape Ag_3Sn near Sn–36Pb–2Ag ball bonding interface cooled at 200 K/min contributed to U_1 descent at $Z = 0\,\mu m$.

(4) U_1 at $Z = 200\,\mu m$ of Sn–36Pb–2Ag ball bonding

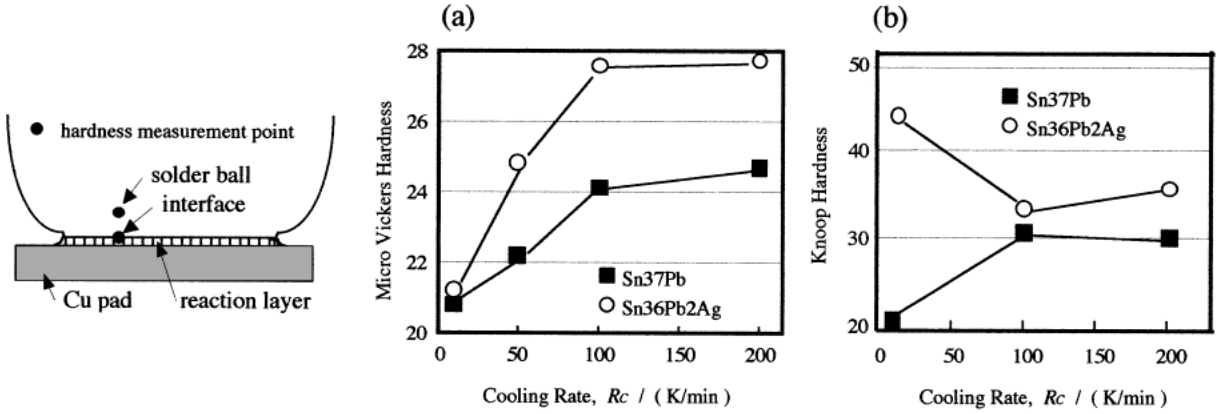

Fig. 14 Relation of cooling rate and micro Vickers hardness of the ball (a) and Knoop hardness of the bonding interface (b).

cooled at 10 K/min–200 K/min was higher than that of Sn–37Pb ball bonding.

(5) The higher U_1 at $Z = 200\,\mu m$ of Sn–36Pb–2Ag ball bonding cooled at each cooling rate was due to the ball hardness.

(6) U_2 was independent on the cooling rates, the ball composition and the shear height.

REFERENCES

1) T. Akamatsu, Y. Yamagishi, K. Imamura, O. Yamaguchi and M. Minamizawa: Proc. 2001 Int. Symposium on Microelectronics, (The Int. Microelectronics and Packaging Society, Washington, DC, 2001) pp. 547–552.
2) K. Jonnalagadda, T. Bai and B. Olson: Proc. 2001 Int. Symposium on Microelectronics, (The Int. Microelectronics and Packaging Society, Washington, DC, 2001) pp. 553–558.
3) S. Popelar, A. Strandjord and B. Niemet: Proc. 2001 Int. Symposium on Microelectronics, (The Int. Microelectronics and Packaging Society, Washington, DC, 2001) pp. 575–580.
4) Z. S. Karim and J. Martin: Proc. 2001 Int. Symposium on Microelectronics, (The Int. Microelectronics and Packaging Society, Washington, DC, 2001) pp. 581–587.
5) M. E. Loomans, S. Vaynman, G. Ghosh and M. E. Fine: J. Electron. Mater. **23** (1994) 741–746.
6) J. Takemoto: J. Metals **45** (1993) 13–40.
7) T. Nishina and K. Okamoto: Proc. 2001 Int. Symposium on Microelectronics, (The Int. Microelectronics and Packaging Society, Washington, DC, 2001) pp. 535–540.
8) S. Nomura, M. Miyazaki, K. Oki, A. Yoshida, S. Ogata and T. Takei: Proc. 2001 Int. Symposium on Microelectronics, (The Int. Microelectronics and Packaging Society, Washington, DC, 2001) pp. 541–546.
9) T. Akamatsu, Y. Yamaguchi, K. Imamura, O. Yamaguchi and M. Minamizawa: Proc. 2001 Int. Symposium on Microelectronics, (The Int. Microelectronics and Packaging Society, Washington, DC, 2001) pp. 547–552.
10) K. Uenishi, T. Saeki, Y. Kohara, K. F. Kobayashi, I. Shoji, M. Nishiura and M. Yamamoto: Mater. Trans. **42** (2001) 756–760.
11) P. L. Tu, Y. Chan, K. C. Humg and J. K. L. Lai: IEEE Trans **23** (2000) 750–756.
12) K. Noguchi, M. Ikeda, I. Shimizu, Y. Kawamura and Y. Ohno: Mater. Trans. **42** (2001) 761–768.
13) K. Noguchi, M. Ikeda, I. Shimizu, Y. Ohno and T. Nakamori: Submitting to Materials Transactions.
14) K. Noguchi, M. Araki and Y. Ohno: Scr. Mater. **43** (2000) 199–204.
15) K. Noguchi, M. Araki, E. Imazato, I. Shimizu and Y. Ohno: Journal of the Japan Welding Society **18** (2000) 600–605.